16th World Conference on Earthquake Engineering, 16WCEE 2017

Santiago Chile, January 9th to 13th 2017

Paper N° 1953

Registration Code: S-K1463148816

Advanced reliability method applied to a hybrid seismic test of a retrofitted motorway bridge

F. J. Molina [1], P. Pegon [2], M. Poljansek [3], F. Taucer [4]

[1] *Deputy Head of Laboratory, European Commission, Joint Research Centre (JRC), francisco.molina@jrc.ec.europa.eu*
[2] *Head of Laboratory, European Commission, Joint Research Centre (JRC), pierre.pegon@jrc.ec.europa.eu*
[3] *Project Leader, European Commission, Joint Research Centre (JRC), martin.poljansek@jrc.ec.europa.eu*
[4] *Policy Officer, European Commission, Joint Research Centre (JRC), fabio.taucer@ec.europa.eu*

…

Abstract

An upgraded hybrid cyber-physical technique was introduced to assess the seismic response of a reinforced concrete motorway bridge and the effectiveness of the friction-pendulum seismic isolation. The two independent roadway bridge was built in the 1960s in Italy and it spans over twelve couples of portal frame piers. Two of the piers (scale 1:2.5) and two seismic isolators setups detached from the piers were constructed at the European Laboratory for Structural Assessment (ELSA). Altogether eighteen actuators where installed, of which six controlled horizontal displacements and twelve ensured vertical loading on the piers and isolators.

To obtain the dynamic response of the whole bridge, the part not present physically in the laboratory was modelled numerically. In the upgraded cyber-physical technique, two processes were running in parallel, one for the numerical model and the other controlling the motion of the physical model in the laboratory. These two processes had different time steps and ran two different time integration schemes. This way the physical structures were in continuous movement following an explicit time integration scheme whereas the numerical model could have a huge number of degrees of freedom and high non-linearity and use the implicit time integration scheme.

The deleterious effect of control errors in the obtained response for the hybrid test was quantified by assessing the frequency and damping distortion in the obtained response as identified from equivalent numerical models. The models were based only on the measurements done during the experiment, which increases the generality and applicability of the reliability assessment method.

Keywords: Hybrid testing, Bridge retrofit, Base isolation, Error control, Reliability assessment

1 Introduction

In a hybrid cyber-physical test campaign at the European Laboratory for Structural Assessment (ELSA) of the European Commission's Joint Research Centre, the seismic response of a reinforced concrete (RC) motorway bridge was studied [1]. Performances of the as-built and retrofitted bridge were compared in order to assess the advantages and limitations of the seismic friction-pendulum deck isolation.

The studied motorway bridge, Fig. 1a, was built in the 1960s between Florence and Bologna in Italy. 12 couples of portal frame piers support the deck with two independent roadways. The circular piers are 120 to 160 cm in diameter and connect at the top with a cap-beam and with one or more transverse beams of rectangular sections. The deck is simply supported on the beams and is anchored with steel bars without seismic isolation.

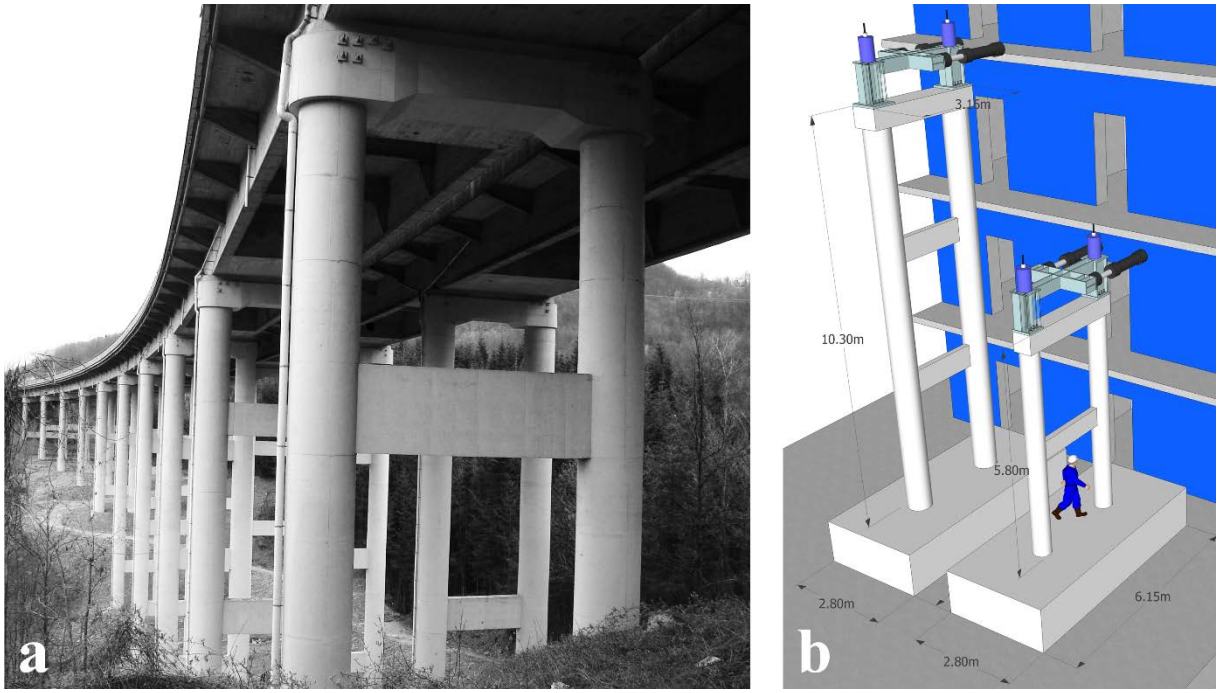

Fig. 1 – a: Rio-Torto bridge, b: Test set-up of the piers 9 and 11 scaled at 1:2.5 in ELSA

One short and one tall piers were selected as physical models for the hybrid test campaign. The two selected piers were identified in numerical simulations of the seismic response of the existing bridge because the flexural failure of columns and widespread shear brittle ruptures in their transverse beams.

The test rig configuration used for the two 1:2.5 scaled piers installed next to the reaction wall of ELSA, Fig. 1b. The effect of the deck on the piers was simulated with steel interface loading frames to which horizontal and vertical loads were applied by hydraulic actuators. Hybrid tests on the bridge retrofitted with seismic isolation located between the top of the piers and the bridge deck were implemented with a sub-structuring method. The proposed isolation system consisted of four friction pendulum isolators per pier, which, in the setup at the laboratory, were located at the ground level, Fig. 2.

Numerical simulations of the prototype bridge were carried out to predict the earthquake response of the structural system and optimize the selection of the experimental tests to perform on the as-built and seismically

isolated viaducts [2]. Refined and simplified finite element (FE) models were thus implemented. In the refined model, the bridge response was simulated numerically by using the non-linear OpenSees code.

For the ultimate reliability of the test results an assessment criteria was introduced where obtained experimental eigenfrequencies and damping ratios were compared with the ones of an ideal prototype structure (in this case equivalent to the same experimental setup but without control errors). Those frequencies and damping ratios are estimated by means of linear models that approximate both the experimental system and the prototype one and are always identified exclusively from the results of the test in question, assuming that all the excitations really acting on the specimen during the test are properly measured.

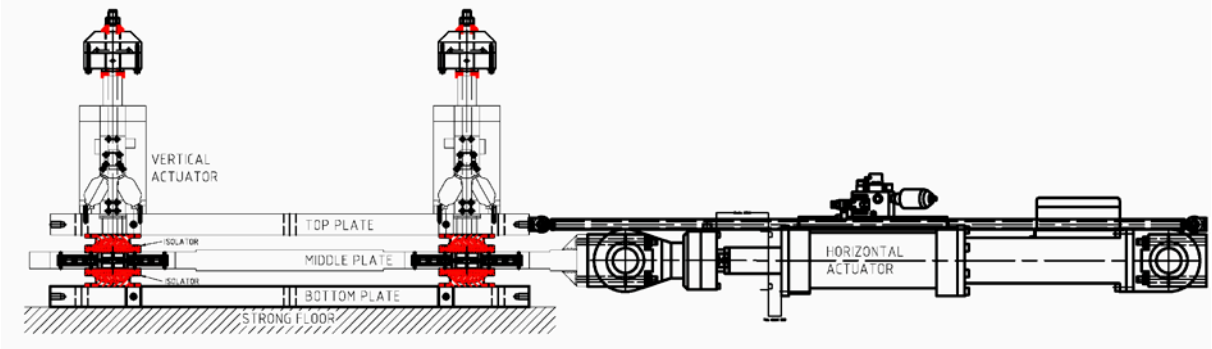

Fig. 2 - Side view of the isolator set-up

2 Advanced hybrid test method

The combination of eighteen servo controlled actuators of the physical model, a refined non-linear numerical model of the piers and isolators with a large number of degrees-of-freedom (DoF) required an advanced hybrid test method with a robust equilibrium iteration that also allowed model updating [2].

In the applied advanced hybrid test method two processes run in parallel. The first one is responsible for the numerical structure and the second one controls the motion of the physical structure in the lab, preserving the smooth character of the continuous hybrid test method. These two process had different time steps because it is virtually impossible to ensure that, within the laboratory time step of 2 ms, the refined nonlinear numerical process can be completed. Furthermore, two different time integration schemes were run. The conditional stability of the laboratory explicit central difference scheme requires much less computation time than the numerical structure utilizing the implicit scheme to manage the larger time step and the larger number of DoFs. Starting from the domain decomposition scheme presented in [3], it was shown that it is possible to transform a staggered asynchronous procedure in an inter-field parallel procedure suitable to work with one synchronous process, keeping most of the original characteristics of the scheme [4]. For the non-linear case, a combination of a non-iterative Operator Splitting strategy [5], [6] and of a non-linear condensation technique was proposed to handle the analytical structure [7]. This distributed scheme was described in [8], and a convergence analysis was made in [9]. However, in the present campaign, the specimens are much larger and are exposed to accumulated severe damage. In order to maintain the same standards for error of the state-of-the-art continuous hybrid testing at ELSA, it was thus needed to substantially upgrade the substructuring implementation of 2005.

As with all substructured tests performed at ELSA, the software used for the numerical part was Cast3M [10], a multi-purpose finite element code which was slightly modified in order to introduce the non-linear models used during the tests.

3 Assessment of reliability of the hybrid test

The method described here is based on the approach presented in [11], by which the reliability of a test in the presence of control errors can be assessed. There, the testing setup is understood as the experimental model

of an ideal prototype system (characterised by a functional operator $F\{\ \ \}$) through which the specified input $i(t)$ gives the ideal output $o(t)$

$$o(t) = F\{i(t)\} \tag{1}$$

For this purpose, the 'prototype system' is defined as the same as the experimental setup but without any control error. In contrast to Eq. (1), due to the presence of the control errors, in the experimental setup, we have a performed input $i^{perf}(t)$ that produces the performed output $o^{perf}(t)$ through the experimental functional operator $F^{exp}\{\ \ \}$. That is,

$$o^{perf}(t) = F^{exp}\{i^{perf}(t)\} \tag{2}$$

Typically, for pseudo-dynamic and hybrid tests, the input is the ground accelerogram or applied external forces that enter directly in the numerical equation of motion without distortion. In that case, the proposed assessment of the reliability of the test is preferably based on the comparison check of the experimental operator with the prototype operator, i.e.,

$$F^{exp}\{\ \ \} \approx\ F\{\ \ \}\ \ ? \tag{3}$$

rather than on the comparison of the performed output with its relative ideal output, which would be more limitative. More specifically, conceptually, the comparison of the operators Eq. (3) is done by looking at an equivalent linear case based on a linear specimen which eigenfrequencies and damping ratios are distorted by passing from the prototype case to the experimental setup. In a way, the approach is similar to the one typically used for stability and accuracy analysis of step-by-step time-integration numerical methods that is based on the observation of the distortion in frequency and damping for the performed modes of a linear specimen, [12]. In practice, we will perform an identification of an equivalent linear system at different time intervals of the experimental response. The identification will render eigenfrequency and damping ratio values for the prototype system as well as for the experimental system showing their evolution in the time and the distortion introduced by the control errors.

3.1 Formulation for the case of a hybrid test with substructuring

3.1.1 Equation of motion of the prototype system

We will assume that the ideal global system corresponds to the prototype equation of motion

$$\boldsymbol{M}\ddot{\boldsymbol{d}}_{\boldsymbol{G}}(t) + \boldsymbol{r}_{\boldsymbol{G}}(t) = -\boldsymbol{M}\boldsymbol{J}\boldsymbol{a}_{\boldsymbol{g}}(t) \tag{4}$$

where the global restoring force vector is composed by equilibrium from the restoring force vectors of the numerical (called A) and the experimental (physical) substructure (called B):

$$\boldsymbol{r}_{\boldsymbol{G}}(t) = \boldsymbol{T}_{\boldsymbol{G}}^{\boldsymbol{A}}\boldsymbol{r}_{\boldsymbol{A}}(t) + \boldsymbol{T}_{\boldsymbol{G}}^{\boldsymbol{B}}\boldsymbol{r}_{\boldsymbol{B}}(t) \tag{5}$$

Here $\boldsymbol{T}_{\boldsymbol{G}}^{\boldsymbol{A}}$ and $\boldsymbol{T}_{\boldsymbol{G}}^{\boldsymbol{B}}$ are constant matrices that include the connectivity of the DoFs of the substructures and, in the case of $\boldsymbol{T}_{\boldsymbol{G}}^{\boldsymbol{B}}$, their implemented scale in the setup.

From the global displacements $\boldsymbol{d}_{\boldsymbol{G}}(t)$, the corresponding vectors of displacement at the substructures are derived as:

$$\boldsymbol{d}_{\boldsymbol{A}}(t) = \boldsymbol{T}_{\boldsymbol{A}}^{\boldsymbol{G}}\boldsymbol{d}_{\boldsymbol{G}}(t), \quad \boldsymbol{d}_{\boldsymbol{B}}(t) = \boldsymbol{T}_{\boldsymbol{B}}^{\boldsymbol{G}}\boldsymbol{d}_{\boldsymbol{G}}(t) \tag{6}$$

where the matrices, by reciprocity, can be obtaining by transposing

$$\boldsymbol{T_A^G} = \left(\boldsymbol{T_G^A}\right)^{\boldsymbol{T}}, \quad \boldsymbol{T_B^G} = \left(\boldsymbol{T_G^B}\right)^{\boldsymbol{T}} \tag{7}$$

In order to obtain the estimates of the eigenvalues of the prototype system and the hybrid test system, the Spatial Model identification method will be applied [13], [14], [15].The Spatial Model assumes that the restoring force can be modelled by an equivalent linear system of the form

$$\boldsymbol{r_G}(t) = \boldsymbol{K}\boldsymbol{d_G}(t) + \boldsymbol{C}\dot{\boldsymbol{d}}_{\boldsymbol{G}}(t) \tag{8}$$

where, for a short time interval, $\boldsymbol{K}$ and $\boldsymbol{C}$ are constant matrices of stiffness and damping. If the displacements, velocities and forces in Eq. (8) are known, the method consists of using a time-window of data centred at selected regular time instants and apply least-square identification on the coefficients of $\boldsymbol{K}$ and $\boldsymbol{C}$. Once these two matrices are identified, they are combined with the theoretical mass matrix $\boldsymbol{M}$ appearing in Eq. (4) in order to formulate the eigenvalue problem

$$s\begin{bmatrix}\boldsymbol{C} & \boldsymbol{M}\\ \boldsymbol{M} & \boldsymbol{0}\end{bmatrix}\boldsymbol{\phi} + \begin{bmatrix}\boldsymbol{K} & \boldsymbol{0}\\ \boldsymbol{0} & -\boldsymbol{M}\end{bmatrix}\boldsymbol{\phi} = \boldsymbol{0} \tag{9}$$

that has as solution the conjugate eigenmode couples with respective eigenvalue couples

$$\boldsymbol{\phi_i}, \boldsymbol{\phi_i}^*; \quad s_i, {s_i}^* = \omega_i\left(-\zeta_i \pm j\sqrt{1-{\zeta_i}^2}\right) \tag{10}$$

where ω_i is the natural frequency and ζ_i is the damping ration for mode $\boldsymbol{\phi_i}$.

3.1.2 Identification of the performed natural frequencies and damping ratios

More precisely, during the hybrid test, the equation of motion is approximately solved by the adopted combined discrete-time algorithms of the numerical and the physical substructures (A and B). If we assume that the numerical error introduced by those algorithms is negligible for the adopted integration time increments, the performed response during the test would be equivalent to the solution of the global setup equation of motion

$$\boldsymbol{M}\ddot{\boldsymbol{d}}_{\boldsymbol{G}}^{\boldsymbol{perf}}(t) + \boldsymbol{r_G}^{\boldsymbol{perf}}(t) = -\boldsymbol{M}\boldsymbol{J}\boldsymbol{a_g}(t) \tag{11}$$

where the control errors are responsible for the difference with respect to the prototype system Eq. (4). By applying the Spatial Model to the performed global displacements $\boldsymbol{d_G}^{\boldsymbol{perf}}(t)$ and performed restoring forces $\boldsymbol{r_G}^{\boldsymbol{perf}}(t)$

$$\begin{gathered}\boldsymbol{r_G}^{\boldsymbol{perf}}(t) = \boldsymbol{K}^{\boldsymbol{perf}}\boldsymbol{d_G}^{\boldsymbol{perf}}(t) + \boldsymbol{C}^{\boldsymbol{perf}}\dot{\boldsymbol{d}}_{\boldsymbol{G}}^{\boldsymbol{perf}}(t)\\ \xrightarrow{\textbf{Least Square}} \boldsymbol{K}^{\boldsymbol{perf}};\ \boldsymbol{C}^{\boldsymbol{perf}}\end{gathered} \tag{12}$$

the performed global stiffness $\boldsymbol{K}^{\boldsymbol{perf}}$ and damping $\boldsymbol{C}^{\boldsymbol{perf}}$ are identified. This allows formulating the eigenvalue problem which solution are the performed natural frequencies and damping ratios

$$\begin{gathered}s\begin{bmatrix}\boldsymbol{C}^{\boldsymbol{perf}} & \boldsymbol{M}\\ \boldsymbol{M} & \boldsymbol{0}\end{bmatrix}\boldsymbol{\phi} + \begin{bmatrix}\boldsymbol{K}^{\boldsymbol{perf}} & \boldsymbol{0}\\ \boldsymbol{0} & -\boldsymbol{M}\end{bmatrix}\boldsymbol{\phi} = \boldsymbol{0}\\ \xrightarrow{\boldsymbol{eigenvalue}} {\omega_i}^{perf};\quad {\zeta_i}^{perf}\end{gathered} \tag{13}$$

It must be noted that for the linearized experimental performed system Eq. (12), the performed force $\boldsymbol{r_G}^{\boldsymbol{perf}}(t)$ is correlated to the performed displacement and velocity solved by the integration algorithm. However, since the control cannot be perfect, the performed displacement $\boldsymbol{d_G}^{\boldsymbol{perf}}(t)$ that was sent as reference to the control for the deformation of the physical substructure as

$$\boldsymbol{d_B}^{\boldsymbol{perf}}(t) = \boldsymbol{T_B^G}\boldsymbol{d_G}^{\boldsymbol{perf}}(t) \tag{14}$$

must differ from the measured displacements $\boldsymbol{d_B}^{\boldsymbol{meas}}(t)$ in the amount of the control error

$$\boldsymbol{\varepsilon}(t) = \boldsymbol{d_B}^{\boldsymbol{meas}}(t) - \boldsymbol{d_B}^{\boldsymbol{perf}}(t) \tag{15}$$

This allows formulating the Spatial Model restricted to the physical substructure in order to derive its performed stiffness and damping that will be used in the following section

$$\begin{gathered}\boldsymbol{r_B}^{\boldsymbol{perf}}(t) = \boldsymbol{K_B}^{\boldsymbol{perf}}\boldsymbol{d_B}^{\boldsymbol{perf}}(t) + \boldsymbol{C_B}^{\boldsymbol{perf}}\dot{\boldsymbol{d}}_{\boldsymbol{B}}^{\boldsymbol{perf}}(t) \\ \xrightarrow{\textit{Least Square}} \boldsymbol{K_B}^{\boldsymbol{perf}};\ \boldsymbol{C_B}^{\boldsymbol{perf}}\end{gathered} \tag{16}$$

This means that the physical substructure, due to the control errors, appears in a distorted manner by these performed matrices that are associated to distorted frequencies and damping ratios Eq. (13).

3.1.3 Identification of the prototype natural frequencies and damping ratios

We will assume that, for the physical substructure B, the prototype stiffness and damping matrices $\boldsymbol{K_B}$ and $\boldsymbol{C_B}$ can be obtained by applying the Spatial Model to the performed forces and measured displacements

$$\begin{gathered}\boldsymbol{r_B}^{\boldsymbol{perf}}(t) = \boldsymbol{K_B}\boldsymbol{d_B}^{\boldsymbol{meas}}(t) + \boldsymbol{C_B}\dot{\boldsymbol{d}}_{\boldsymbol{B}}^{\boldsymbol{meas}}(t) \\ \xrightarrow{\textit{Least Square}} \boldsymbol{K_B};\ \boldsymbol{C_B}\end{gathered} \tag{17}$$

Note that, as a difference with respect to Eq. (16), in Eq. (17) the displacements correspond to the physical deformation observed in the structure that is directly related to the forces independently of the magnitude of the control errors. On the other hand, for the numerical substructure, since it is not affected by the control errors, it is understood that

$$\boldsymbol{K_A} = \boldsymbol{K_A}^{\boldsymbol{perf}};\qquad \boldsymbol{C_A} = \boldsymbol{C_A}^{\boldsymbol{perf}} \tag{18}$$

Now, by combining expressions Eq. (5), Eq. (6), and Eq. (8), it can be derived that

$$\boldsymbol{K} = \boldsymbol{T_G^A}\boldsymbol{K_A}\boldsymbol{T_A^G} + \boldsymbol{T_G^B}\boldsymbol{K_B}\boldsymbol{T_B^G} \tag{19}$$

And, similarly after Eq. (12),

$$\boldsymbol{K}^{\boldsymbol{perf}} = \boldsymbol{T_G^A}\boldsymbol{K_A}^{\boldsymbol{perf}}\boldsymbol{T_A^G} + \boldsymbol{T_G^B}\boldsymbol{K_B}^{\boldsymbol{perf}}\boldsymbol{T_B^G} \tag{20}$$

Now, by comparing Eq. (19) and Eq. (20) and having into account Eq. (18),

$$\boldsymbol{K} = \boldsymbol{K}^{\boldsymbol{perf}} + \boldsymbol{T_G^B}\left(\boldsymbol{K_B} - \boldsymbol{K_B}^{\boldsymbol{perf}}\right)\boldsymbol{T_B^G} \tag{21}$$

Or in a similar manner for the damping

$$\boldsymbol{C} = \boldsymbol{C}^{\boldsymbol{perf}} + \boldsymbol{T_G^B}\left(\boldsymbol{C_B} - \boldsymbol{C_B}^{\boldsymbol{perf}}\right)\boldsymbol{T_B^G} \tag{22}$$

By using these estimates of the stiffness and damping matrices, the eigenvalue equations Eq. (9) can be formulated and the prototype natural frequencies and damping ratios are solved as

$$s\begin{bmatrix}\boldsymbol{C} & \boldsymbol{M}\\ \boldsymbol{M} & \boldsymbol{0}\end{bmatrix}\boldsymbol{\phi} + \begin{bmatrix}\boldsymbol{K} & \boldsymbol{0}\\ \boldsymbol{0} & -\boldsymbol{M}\end{bmatrix}\boldsymbol{\phi} = \boldsymbol{0} \tag{23}$$

$$\xrightarrow{\boldsymbol{eigenvalue}} \omega_i\,; \quad \zeta_i$$

Then the comparison check of these prototype characteristic values Eq. (23) with the performed ones Eq. (13)

$$\omega_i{}^{perf} \approx \omega_i \quad ???; \quad \zeta_i{}^{perf} \approx \zeta_i \quad ??? \tag{24}$$

allows to give an assessment of the reliability of the executed hybrid test.

3.2 Application to one of the performed experiments

The most deleterious effect of the control errors in the response to a hybrid test typically comes from the delay error in the actuators that has the effect of producing out-of-phase performed forces with respect to the performed displacements. This effect can be assessed by the described approach based on the Spatial Model by looking at the damping ratio of the relevant modes and how much it differs when identified either from the reference (performed) displacements or from the measured displacements. Since the method is better based on the results of an experiment already performed, normally a reduced input non-damaging experiment is done initially that allows to perform this assessment as well as some others regarding the quality of the results. After this check on the non-damaging experiment has been passed, the effect of the control errors on the larger tests is expected to be less significant because, assuming that the servo-valves are far from saturation,

1. The natural frequencies tend to be lower and the out-of-phase effect due to the delay of the actuators becomes proportionally smaller.
2. The damping ratios of the prototype system tend to be higher, which reduces the importance of the damping distortion induced by the control errors.

On the other hand, the application of the Spatial Model to large-input experiments sometimes may produce not so clear results due to the difficulty of identifying a linear system from a strongly non linear response.

In this section we will show the results of the application of the Spatial Model technique to one of the preliminary reduced-input experiments on the RETRO hybrid testing setup. Two experiment runs (called k05 and k06) corresponded to the application of 10% of the SLS (Serviceability Limit State) accelerogram on the non-isolated bridge configuration. The accelerogram was digitized with a time increment of 5 ms, which coincided with the time increment used for the implicit time algorithm applied at the numerical substructure. For the physical substructure using the explicit algorithm, the time increment was 250 or 500 (k05 or k06 respectively) times smaller using 2ms of real time for each one. This means that 5 ms of prototype time were run in $250 \times 2 = 500\,ms$ or $500 \times 2 = 1000\,ms$ (k05 or k06 respectively) of real time and, consequently, the time scale factor was $\lambda = 100$ or $\lambda = 200$ (k05 or k06 respectively). Another difference between the experiment runs was that run k05 was executed for 25 s, whereas run k06 was executed for only 12.5 s of the prototype time.

The Spatial Model identification was applied with the results sampled with the original time increment of 5 ms and using a window with a width of 1000 points (5 s duration) for every identification. Then the results of identified natural frequency and damping ratio are represented at the central time for every identification window in the graphs in Fig. 3 and Fig. 4. For every one of the first six modes in these figures, either for the identified values from the reference displacements (performed system estimate) and the measured ones (prototype system estimate), the left graph shows the natural frequency and the right one the damping ratio as time histories for the two runs of the experiment. The maximum response of the physical piers at the laboratory scale was less than 3 mm, which presents a difficulty for the quality of the results in the presence of the

experimental noise at the signals, especially for the measured forces. However, the obtained curves in Fig. 3 and Fig. 4 give a good estimate of the linear equivalent modal frequencies and damping ratios at the central interval of the response, where the displacement were more significant.

Particularly, from the interval from 7.5 to 15s, for run k05, the average value of frequency and damping derived from the measured displacements Eq. (23) is displayed for modes 1 to 6 in Table 1 at the columns relative to the Spatial Model identifications. In the same table, the difference between the averages of identified values from the measured displacements and from the reference (performed) displacements Eq. (13), divided by the first one, is also displayed as percentage of relative error either for the eigenfrequency or for the damping ratio. Additionally, by substituting in the numerical model used for the hybrid test the physical piers by similar models to the other piers, the obtained modes based on the initial stiffness had associated frequencies and modal masses (as percentage of the total mass) that are displayed in Table 1 at the columns relative to the FEM characteristics. It must be noted that, according to the modal masses computed by the FEM, more than 99% of the total mass is represented by these first six modes. The frequencies of these six modes from the FEM are well reproduced by the Spatial Model identification. This was not the case for everyone the remaining modes (not displayed) probably due to their small participation in the response that makes not reliable the identification from the experimental results.

Regarding the assessment of the effects of the control errors, we can say that the relative errors are very small either for the eigenfrequencies or for most of the damping ratios. The relative error in damping for mode 4, being higher, is in the order of 5%, which this is acceptable since the modal mass of this mode represents only one fifth of the total mass. On the other hand, this error does not seem to be explained by the delay of the actuators since, by reducing the testing speed to one-half from run k05 to run k06, the magnitude of the error did not improve (see the top right graph in Fig. 4).

Table 1 - average value of frequency and damping

	FEM		Spatial Model (for k05 applied to interval from 7.5 to 15s)			
	Modal mass/ Total mass	Eigen freq	Eigen freq	Freq Rel Err	Damp Ratio	Damp Rel Err
Unit	%	Hz	Hz	%	%	%
Mode 01	13.42	0.600	0.594	-0.003	5.66	-0.13
Mode 02	43.65	0.615	0.615	0.000	4.89	0.01
Mode 03	8.42	0.649	0.649	0.002	4.91	-0.06
Mode 04	22.78	1.028	0.976	-0.076	5.80	5.61
Mode 05	6.24	1.100	1.103	0.001	5.09	0.00
Mode 06	4.73	1.282	1.286	-0.001	5.11	0.08
	Σ=99.23					

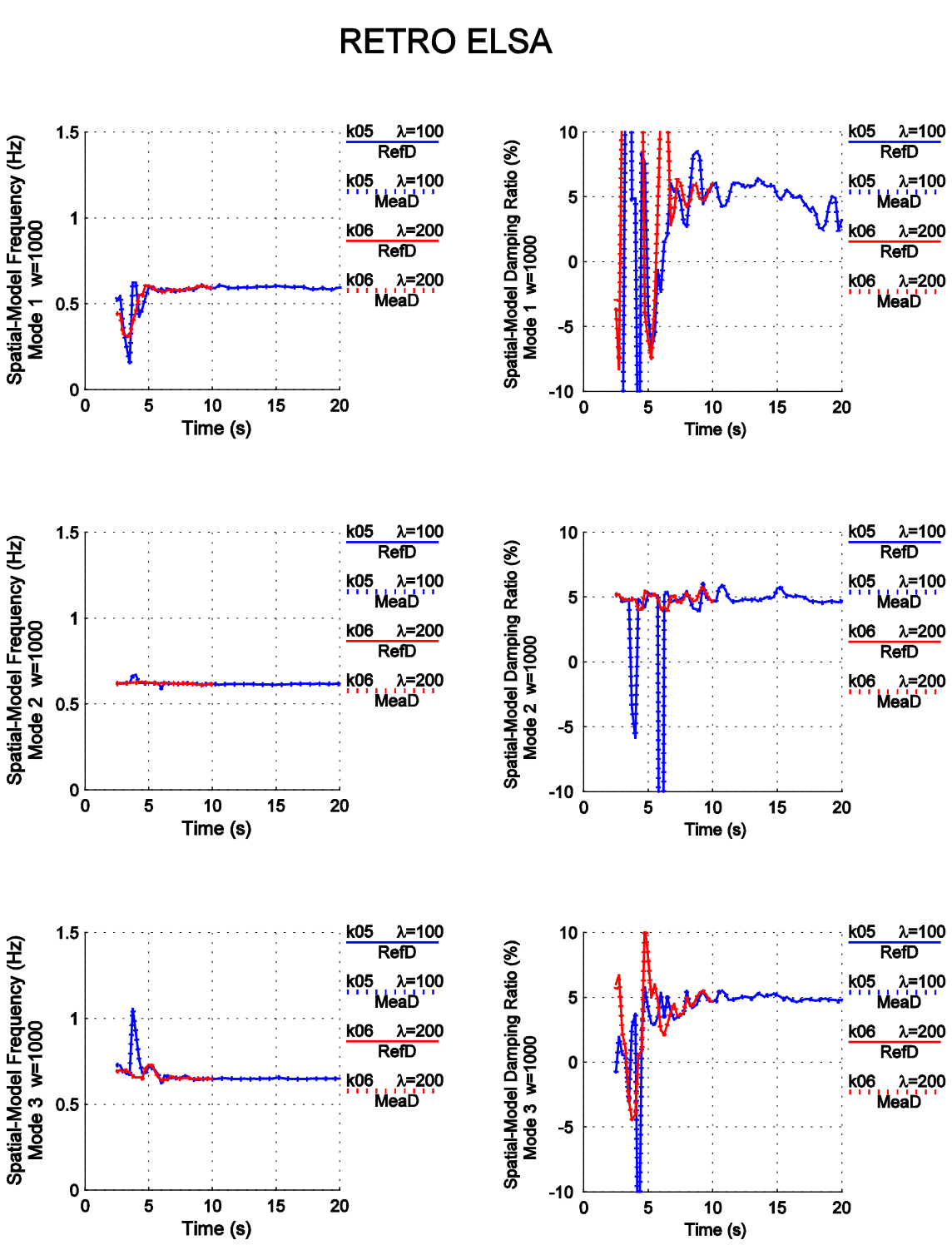

Fig. 3 - Comparison of identified natural frequencies and damping ratios for the prototype and the performed system at modes 1, 2 and 3.

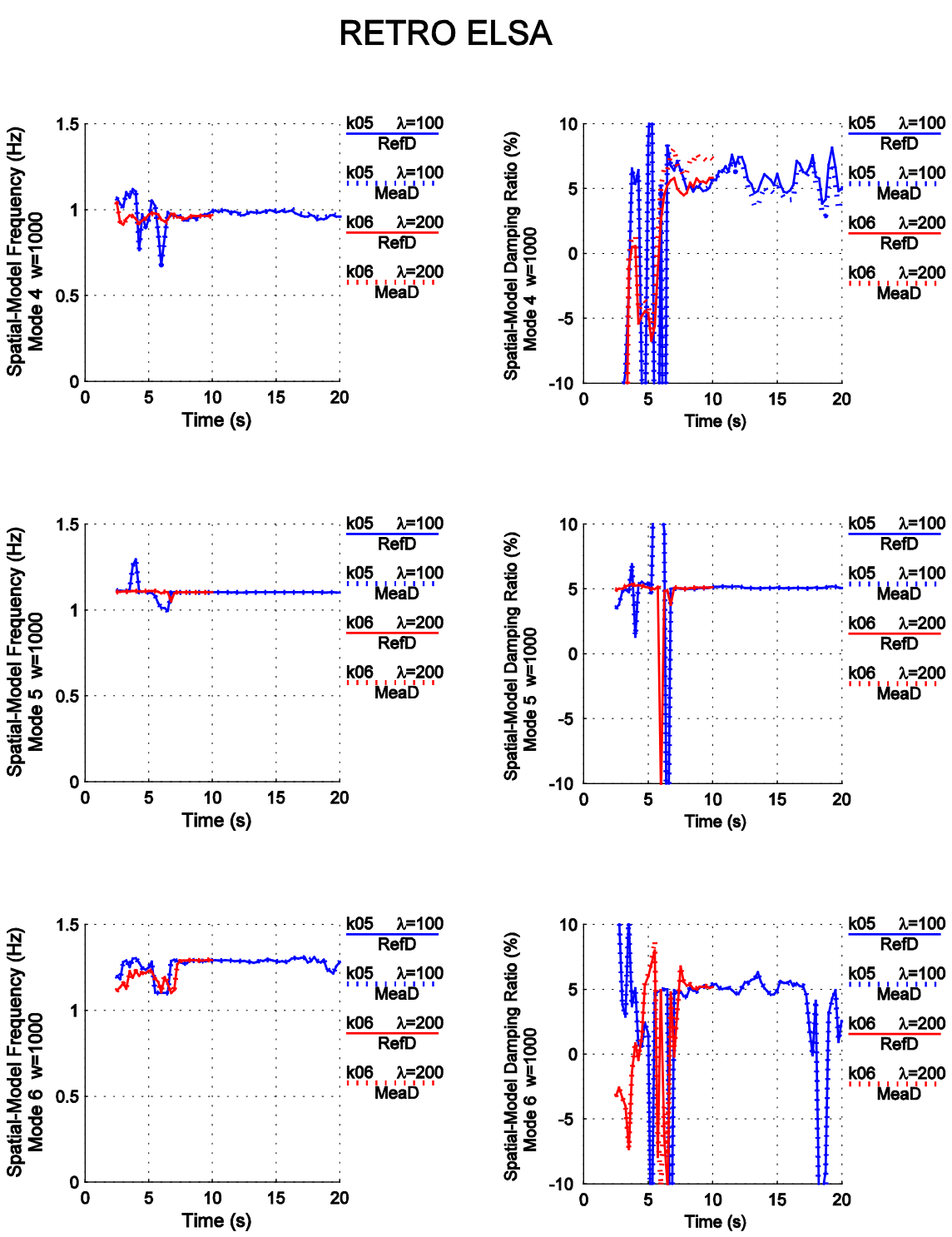

Fig. 4 - Comparison of identified natural frequencies and damping ratios for the prototype and the performed system at modes 4, 5 and 6.

CONCLUSIONS

The dynamic response of the large motorway bridge in as-built and retrofitted configuration was studied in an advanced hybrid test campaign. Two out of twelve bridge piers were physically installed in ELSA together with two seismic isolator setups. The upgraded hybrid method, with two processes having different time steps and time integration schemes, has proven to perform accurately. One process was the nonlinear numerical model of the bridge and the other was controlling the continuous motion of the physical model. Furthermore, it was shown that large, highly nonlinear physical models with many DoF can be reliably and safely tested at ELSA.

The applied Spatial Model identification for the natural frequencies and damping ratios of the bridge, based on the obtained response and the measured control errors, has been applied at different successive time instants and has produced time histories of such characteristic values for a test example. These results have allowed to assess the negligible effect of those errors in the distortion of frequency and damping for the relevant modes in the response.

REFERENCES

[1] Paolacci F, Pegon P, Molina FJ, Poljansek M, Giannini R, Di Sarno L, Abbiati G, Mohamad A, Bursi O, Taucer F, Ceravolo R, Zanotti Fragonara L, De Risi R, Sartori M, Alessandri S, Yenidogan C (2014). Assessment of the seismic vulnerability of an old RC viaduct with frame piers and study of the effectiveness of base isolation through PsD testing (RETRO), *Publications Office of the European Union*

[2] Paolacci F; Di Sarno L; Pegon P; Molina FJ; Poljansek M; Bursi OS; Abbiati G; Ceravolo R; Erdik M; De Risi R; Mohamad A (2015): Assessment of the seismic behaviour of a retrofitted old R.C. highway bridge through PsD testing. *Experimental Research in Earthquake Engineering*, 199- 227

[3] Gravouil A, Combescure A (2001). Multi-time-step explicit-implicit method for nonlinear structural dynamics. *International Journal for Numerical Methods in Engineering*, 50:199–225

[4] Pegon P, Magonette G (2002). Continuous PsD testing with non-linear substructuring: presentation of a stable parallel inter-field procedure. *JRC-Special publication* No. *SPI.02.167*

[5] Nakashima M, Akazawa T, Sakaguchi O (1993). Integration method capable of controlling experimental error growth in substructure pseudo dynamic test. *AIJ J Struct Constr Eng* 454:61–71

[6] Combescure D, Pegon P (1997). α-operator splitting time integration technique for pseudodynamic testing: error propagation analysis. *Soil Dyn Earthq Eng* 16:427–443

[7] Pegon P, Magonette G (2005). Continuous PsD testing with non-linear substructuring: using the operator splitting technique to avoid iterative procedures. *JRC-Special publication* No. SPI.05.30

[8] Pegon P (2008). Continuous PsD testing with substructuring. In: Bursi OS, Wagg DJ (eds) *Modern testing techniques for structural systems, dynamics and control* CISM, Italy

[9] Bonelli, A., Bursi, O.S., He, L., Magonette, G., Pegon, P. (2008). Convergence analysis of a parallel interfiled method for heterogeneous simulations with substructuring, *International Journal for Numerical Methods in Engineering*, 75, 7, 800-825

[10] Millard A (1993). CASTEM 2000, Guide dutilisation, *Saclay, France, Rapport*, CEA 93/007

[11] Molina FJ, Pegon P, Magonette G. (2009). Reliability of dynamic and hybrid tests in the presence of control errors. *3rd International Conference on Advances in Experimental Structural Engineering 3AESE Conference Proceedings*, Pacific Earthquake Engineering Research Center, Berkeley.

[12] Hilber, H.M., Hughes, T.J.R., and Taylor, R.L. (1977). Improved numerical dissipation for time integration algorithms in structural dynamics. *Earthquake Engineering and Structural Dynamics,* 5, 283-292.

[13] Molina F. J., Magonette G., Pegon P.& Zapico B. (2011a). Monitoring Damping in Pseudo-Dynamic Tests, *Journal of Earthquake Engineering*, 15:6, 877-900

[14] Molina F. J. (2011b). Spatial and Filter Models, *MATLAB functions available on line at MATWORKS FILE EXCHANGE, The MathWorks, Inc.*, Natick, Massachusetts (USA), August 22,: http://www.mathworks.com/matlabcentral/fileexchange/32634

[15] Molina F. J., Marazzi, F., Viaccoz, B. Bosi, A. (2013). Stability and accuracy in a hybrid test example, *Earthquake Eng. Struct. Dyn.;* 42:469-475.